Inelastic electron scattering by intra- and interband plasmons in rhenium trioxide, tungsten trioxide, and some tungsten bronzes

R. E. Dietz, M. Campagna,* and J. N. Chazalviel†
Bell Laboratories, Murray Hill, New Jersey 07974

H. R. Shanks
Ames Laboratory-ERDA, Iowa State University, Ames, Iowa 50010

(Received 2 September 1977)

Energy-loss spectra were measured by backscattering 500-eV electrons from films of WO_3 grown on single-crystal W(100), and from single crystals of Na_xWO_3 ($0.35 < x < 0.86$) and ReO_3 which were cleaved in ultrahigh vacuum. The spectrum of a crystal with $x = 0.61$ was nearly identical to the surface loss function $\mathrm{Im}[-(\epsilon+1)^{-1}]$ calculated from ϵ measured by optical reflectivity on a crystal with $x = 0.65$. For $x = 0.61$, two plasmons are observed, $\omega_- = 1.90$ eV, and $\omega_+ = 6.5$ eV. ω_- scales approximately as $x^{1/2}$ and is assigned to the conduction-electron resonance. The plasmon lifetime $\tau_p = 1.9\times10^{-15}$ sec determined from the observed linewidth agrees well with a value for the conduction-electron relaxation time $\tau_e = 2.1\times10^{-15}$ sec we obtained from previously reported reflectivity data, but is shorter than a value $\tau_c = 6.7\times10^{-15}$ sec we estimated from previously reported dc conductivity data. The higher-energy plasmon ω_+ is assigned to a screened longitudinal resonance of an interband excitation near 5 eV. ω_+ is essentially independent of x for $0 \le x < 0.9$. By fitting ϵ between 0 and 10 eV with a model dielectric function, we found a value for the mean effective conduction electron mass $m^* = 0.80\ m_e$, the interband contribution to the static dielectric constant $\epsilon_s = 4.35$, and values for parameters characterizing the interband resonance. Taking these latter parameters to be independent of x, we calculated the bulk and surface loss functions for different x values. These calculations indicate that mode hybridization is unimportant for $x < 1$ in the bronzes. The effects of damping or joint density-of-states width, screening, and mode interference on the plasmon spectra are discussed. It is shown that ReO_3 and Ag metal have dielectric and energy-loss functions which are similar to the tungsten bronzes. However, some of the assignments given in the literature as to the identities of the conduction-electron and interband plasmons are interchanged from those given above for the bronzes. We believe that the conduction-plasmon hybridization with interband resonances is less important in those materials than previously realized.

I. INTRODUCTION

ReO_3 and the tungsten bronzes such as Na_xWO_3 constitute an interesting series of d-band metals with high electrical conductivities. While WO_3 is an insulator with an energy gap of the order of 2 eV,[1] the addition of each Na in interstitial sites has the effect of adding an electron to the W $5d$–O $2p\pi$ antibonding conduction band, apparently without significantly hybridizing this band with Na wave functions.[2] Single crystals of metallic Na_xWO_3 are available over a continuous range of $0.25 < x < 1.0$. For $x > 0.5$ the structure is cubic at elevated temperatures, and apparently, slightly distorted in hexagonal and tetragonal forms near room temperature.[3] For lower concentrations, the distortions are larger, but all forms have corner-bonded WO_6 octahedra in common, resulting in a similar band structure. ReO_3 has the cubic perovskite structure similar to the higher-x Na_xWO_3 bronzes, but with 1.0 conduction electron per ReO_3. These compounds present a unique opportunity to study the evolution of the metallic dielectric function over a wide range of conduction-electron densities.

In our experiments, we have probed the dielectric function by scattering electrons with primary energies of a few hundred volts from ultrahigh-vacuum-cleaved single-crystal surfaces of the above described compounds, and observing the energy-loss distributions of the scattered electrons. The response of the metal to the charge-density fluctuation created by the scattering electron is to excite longitudinal resonances which are characterized as plasmons. These resonances appear as complex poles in the energy-loss function. The bronzes[4] and[5] ReO_3 are simple in that below 10 eV the dielectric function is determined by two well-defined oscillators: below 3 eV, there is the Drude-like polarizability from the conduction electron, while near 5 eV there is a strong interband transition arising from the excitation of electrons from the upper part of the valence band to the conduction band.

The bulk or surface energy-loss spectrum of such a metal will contain two peaks in the scattered-electron current versus energy-loss distribution.[6] At low-electron concentrations, the higher-energy peak will be determined by the longitudinal interband resonance, which is screened by

higher-frequency interband contributions to the polarizability. This we shall refer to as the "interband" plasmon. At low energies, there will occur another peak due to the conduction-electron resonance which is screened by the entire low-frequency interband polarizability. This peak is termed the "conduction-electron" or "intraband" plasmon. As the conduction-electron concentration x is increased, the unscreened intraband plasmon energy increases approximately as $x^{1/2}$, and eventually appears at energies greater than the interband resonance. For electron densities such that the intra- and interband plasmon energies are comparable, the plasmons mix[6] or "hybridize" and, as we will show below, interfere.

In this paper, we report electron energy-loss data for WO_3, Na_xWO_3 with $0.3 < x < 0.9$, and ReO_3, and compare these data with surface and bulk energy-loss functions calculated from dielectric data derived from optical-reflectivity measurements.[4,5,7] Using a single damped oscillator for the interband polarizability with semiempirical parameters taken from the optical data, we then calculate the energy-loss spectrum for the Na_xWO_3 bronzes as a function of the electron density x for both surface and bulk plasmons. The calculated spectral features are compared with experiment and discussed with regard to the effects of screening, damping, mixing or hybridization, and interference. Finally, we point out that the phenomenological description of the plasmon resonances in the bronzes also applies to ReO_3 and Ag, suggesting that the previous interpretation[5,8] of these systems should be modified.

II. EXPERIMENT

A. Samples

1. WO_3

A single crystal of tungsten metal was oriented with an electropolished (100) face and mounted on a resistance heater in an ultrahigh-vacuum apparatus. The surface was exposed to 300-Torr O_2 while heating to 800 °C, and the growth of an oxide film was monitored by observing the interference colors in reflected light. Epitaxial films of WO_3 were grown of several hundreds of angstroms thickness, after which the crystal was allowed to cool to room temperature, the chamber evacuated to $\sim 6 \times 10^{-10}$ Torr, and electron-energy-loss measurements were carried out. Immediately following the measurements, the crystal was reheated *in vacuo* to 800 °C for 10 min, which allowed the oxygen to partially diffuse into the crystal bulk. Again, the progress could be followed by a change in the interference color. The crystal was then remeasured for electron energy loss, which showed that the annealing step caused a partial reduction of the oxide layer, resulting in metallic behavior.[9] Subsequent reheating and remeasurement cycles were carried out until the conduction-electron density saturated near 0.5 electrons per unit cell, as determined by measurements of the plasmon energy.

2. Na_xWO_3

A number of single crystals of the sodium-tungsten bronzes were grown with x in the range $0.3 < x < 0.9$. The concentration x was determined for each crystal from a powder x-ray measurement of the lattice parameter a, which was related to x via the empirical relation[10] $a = 3.784 + 0.0820x$, where a is expressed in Å. The crystals were all grown[11] by electrolysis of molten mixtures of Na_2WO_4 and WO_3. These crystals were cleaved *in vacuo* at 6×10^{-10} Torr a few minutes prior to measurement. Cleavage of crystals with $x > 0.5$ produced good (100) surfaces. Low-energy-electron-diffraction (LEED) measurements indicated a structure of $(1 \times 2 + 2 \times 1)$ periodicity but it is not known whether this was the result of a surface rearrangement or because of a bulk distortion from the cubic phase.[3] A surface rearrangement would seem to suggest a surface dielectric function which is significantly different from the bulk, but this was not observed in our spectra. For crystals with $x < 0.5$, poor cleavages were experienced, and no LEED patterns could be observed, indicating considerable disorder.

3. ReO_3

A small single crystal was selected from a multicrystalline mass grown by the iodine transport method[12] and cleaved in ultrahigh-vacuum along a (100) plane. No LEED measurements were made. Electron-energy-loss (ELS) measurements were carried out immediately after cleaving.

B. Measurements

Electron-energy-loss measurements were carried out by means of a double-pass cylindrical-mirror electron velocity analyzer with an integral coaxially-mounted electron gun as manufactured by the Physical Electronics Corporation. The primary electron beam was obtained from a thoriated-tungsten filament and was unmonochromatized. The total energy width at half-height of the elastic beam was typically 0.50 eV at beam currents of 20 nA. The primary energy for most experiments was 500 eV, although some measurements were carried out between 20 and 1000 eV. The primary

beam was incident normal to the surface while the scattered electrons were collected at the usual angle of 42.5° from the normal. The pass energy in the analyzer was 15 eV. The electrons from the analyzer were detected using a spiraltron multiplier and the multiplied pulses were counted with conventional pulse-counting electronics. The counts were stored in a multichannel analyzer and the spectrum scanned many times to enhance the signal-to-noise ratio. Raw, unprocessed data are shown in this paper.

Measurements were made immediately after cleaving the crystals to avoid effects due to chemisorption. Although the LEED patterns became smeared after a few hours due to surface contamination, we were not able to detect a change in the ELS spectrum, even when the samples were allowed to stand for several days at pressures of 10^{-9} Torr. We conclude that either the surface dielectric function is not sensitive to chemisorption, or that the scattered electron distributions come mainly from bulk states.

III. RESULTS

A. WO_3

The electron-energy-loss spectra for the oxidized and for the progressively reduced WO_3 film is shown in Fig. 1. The oxidized film data are given at the bottom of the figure, while data for reduced films are given towards the top. There are in general two strong peaks in the energy-loss spectrum below 10 eV: a relatively broad peak at 6.8–7.0 eV, which is independent of the electron concentration, and a strong, sharp peak which increases from zero energy in the case of the oxidized form to about 1.7 eV for the most reduced film. Without further analysis, it is clear that the 6.9-eV peak is an interband plasmon arising from valence-band excitations, while the lower-energy plasmon is to be associated with the conduction electrons. This identification is inverted from that given by Feinleib *et al.* for the case of ReO_3.[5] The lower-energy plasmon peak in these spectra does not appear to be quite as sharp as in comparable spectra in the Na_xWO_3 compounds, probably because of an inhomogeneous electron density in the film. While we did not attempt to determine independently the electron density in the films, by comparing the spectra of the films with those of the Na_xWO_3 crystals for which x is known, we estimate the highest-electron density in the films to be about 0.5 electrons per unit WO_3.

Recently, Ritsko, Witzke, and Deb[13] have reported electron-energy-loss experiments in which 300-keV electrons were transmitted through thin films of WO_3. Their spectra for reduced WO_3 films are somewhat similar to ours, with the differences perhaps due to different chemical treatments in the film preparation.

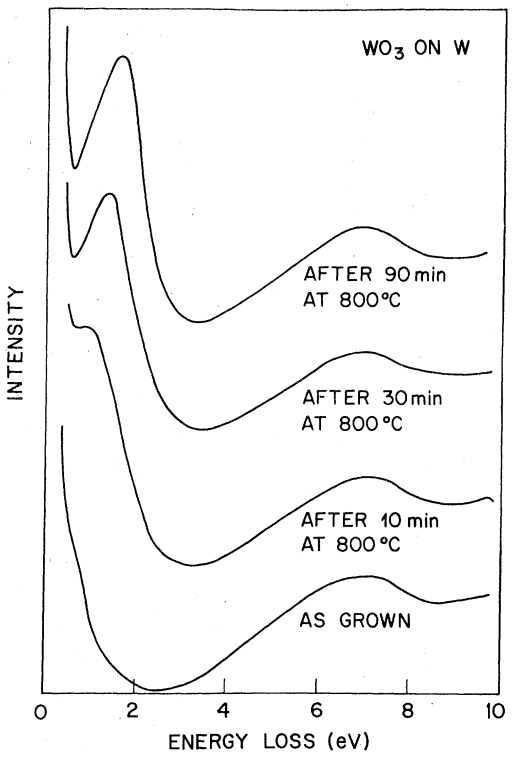

FIG. 1. Electron-energy-loss spectra for a WO_3 film grown by oxidizing a single-crystal W(100) surface. The lowest curve gives the spectrum recorded immediately after growing the WO_3 film. The upper three spectra correspond to various stages of reduction of the film, which was accomplished by heating the film in vacuum. The plasmon near 7 eV is shown to be independent of the conduction-electron density, which causes the lower-energy plasmon to increase in energy.

We concur with Ritsko *et al.* in their interpretation of the 7-eV peak in WO_3 and of the 5.5-eV peak in ReO_3, both of which they assign to an interband transition. On the other hand, they attribute the low-energy peak to a color-center excitation, characteristic of amorphous material, in contrast to our identification of a similar peak in crystalline material as a plasmon, Unfortunately, the resolution of the problem presented by two very similar spectra being explained by quite different models for the excitations is beyond the scope of the present work since we did not investigate amorphous WO_3.

B. Na_xWO_3

The ELS spectra of these compounds are very similar to the spectra of the reduced WO_3 films. The strong, sharp, lower-energy plasmon is x

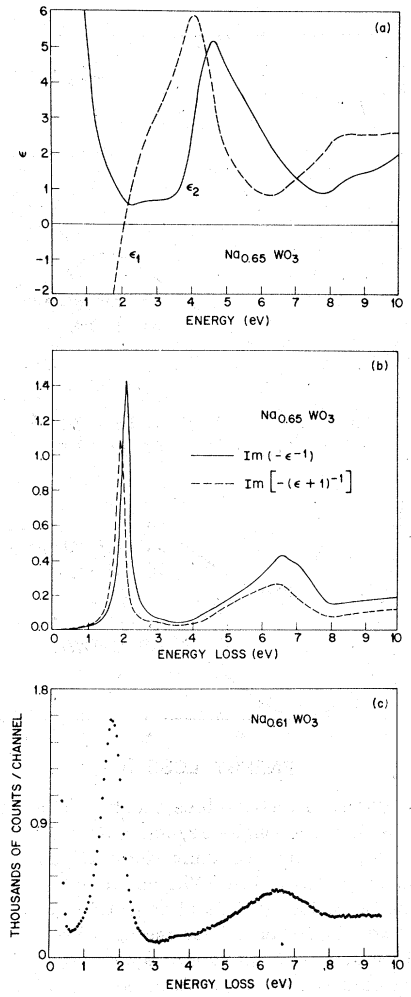

FIG. 2. (a) Bulk dielectric function ϵ obtained by a Kramers-Kronig transformation of optical-reflectance data[4] for $Na_{0.65}WO_3$. (b) Bulk electron energy-loss function $\mathrm{Im}(-\epsilon^{-1})$ and the surface electron energy-loss function $\mathrm{Im}[-(\epsilon+1)^{-1}]$ calculated from ϵ given in (a). (c) Energy-loss spectrum for 500-eV electrons reflected from a vacuum-cleaved (100) surface of $Na_{0.61}WO_3$. The sharp peak at 1.90 eV is ω_-, the conduction-electron plasmon. The broader peak at 6.5 eV is a screened interband longitudinal resonance, while the weak peak at 3.8 eV is $2\omega_-$.

dependent, while the broader, weaker higher-energy plasmon is not. The ELS spectrum for a crystal with $x = 0.61$ is given in Fig. 2(c). The energy of the lower-energy plasmon varies approximately as $x^{1/2}$, as expected for a free-electron plasmon. The positions of the plasmon peaks are plotted versus $x^{1/2}$ in Fig. 7 and compared with a semiempirical calculation to be discussed in Sec. IV. The deviation of the points from a line proportional to $x^{1/2}$ appears to be just outside experimental error, and may indicate an increase in the mean effective conduction-band mass at the higher-electron concentrations. This would be expected on the basis of taking Mattheiss' ReO_3 band-structure calculation[14] to be a rigid-band representation for Na_xWO_3 irrespective of Na concentration. However, the increase in lattice parameter on adding Na may also decrease the p-d overlap at high concentrations sufficiently to observe an increase in the mean effective mass. On the other hand, the insensitivity of the upper plasmon peak to x casts some doubt on this explanation.

The very weak peak observed in Fig. 2(c) near 4 eV is real, and increases somewhat in strength with x. This is a second-order replica of the strong peak near 2 eV, and its observation enables us to compute the constant S for the electron-plasmon interaction, assuming that the intensity is distributed according to the Poisson distribution $I(n) = e^{-S}S^N/N!$. Since the intensity of the second-order peak is about $\frac{1}{50}$ of that of the first-order peak, we obtain $S \sim 0.04$. However, the ratio of the strength of the elastic peak to that of the first-order peak is only about 8, whereas we would predict it to be S^{-1} or about 25.

We also attempted to estimate the full width at half height of the plasmon lines for different values of x. This was difficult to do accurately for either line: For the low-energy line, the observed width, typically 0.68 eV, was just larger than the width of the resolution function, typically 0.50 eV, as estimated from the width of the elastic peak; for the higher-energy line, the width was difficult to estimate because of the background on which it was superposed and because of its asymmetry. Nevertheless, we found that the apparent widths of the two lines were within experimental accuracy independent of x, with the width of the upper line being about 2.0 eV, while the lower line was 0.35 eV, assuming Gaussian shapes for both the plasmon line and the resolution function.

C. ReO_3

As seen in Fig. 3(b), the ELS spectrum of ReO_3 is very similar to the data for $Na_{0.61}WO_3$ given in Fig. 2(c) in the region below 10 eV. A strong, sharp peak is observed at 2.05 eV, and another, broader peak near 5.5 eV. The inelastic spectrum is more weakly scattering relative to the elastic peak in ReO_3 than in Na_xWO_3, with the result that one is unable to detect the second-order peak for the lower-energy plasmon. The fact that S is so small in ReO_3 and in the tungsten bronzes indicates that there is very little multiple inelastic scattering contributing to that part of the spectrum depicted in this paper. The ELS results will be compared to the energy-loss functions calculated

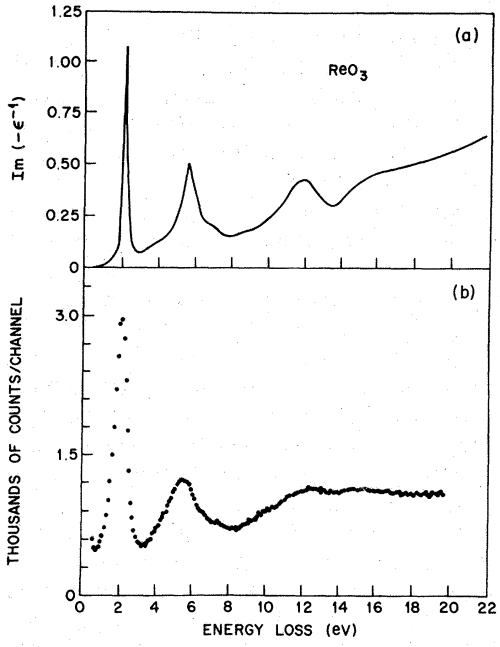

FIG. 3. (a) Bulk electron energy-loss spectrum calculated from optical-reflectivity data (Ref. 5). (b) The energy-loss spectrum obtained by reflecting 500-eV electrons from a vacuum-cleaved (100) surface. The agreement with (a) is excellent, considering that the experimental spectrum is dominated by the surface spectral density.

from the optical reflectivity in the following section.

In the case of ReO_3, the width of the low-energy plasmon is of some interest as well, since Feinleib *et al.*[5] have determined τ independently from dc conductivity, and optical reflectance measurements. We obtain a measured value of 0.80 eV for the full width at half-height, with an elastic peak width of 0.53 eV. Assuming Gaussian shapes (valid for the high-energy-loss side of the elastic peak) we obtain a net width of 0.60 eV for the plasmon.

IV. DISCUSSION

A. Comparison of ELS data with loss functions computed from optical reflectivity

The real and imaginary parts (ϵ_1 and ϵ_2) of the dielectric function for $Na_{0.65}WO_3$ were obtained by Lynch *et al.*[4] by a Kramers-Kronig (KK) transformation of optical reflectance data, and are shown in Fig. 2(a). These data are dominated by the interband transition centered near 5 eV, and the Drude-like conduction-electron response below 3 eV. ϵ_1 has a zero near 2 eV in a region where ϵ_2 is also small, leading to a strong and sharp plasmon in the bulk loss function $\mathrm{Im}(-\epsilon^{-1})$, which was calculated by Lynch *et al.*[4] and is shown in Fig. 2(b). We have calculated the surface loss function $\mathrm{Im}[-(\epsilon+1)^{-1}]$ which is also given in Fig. 2(b), and is very similar to the bulk loss function. The main differences are that the surface-plasmon energies are slightly smaller, and the modes are not as intense. The lower-energy mode, which we will henceforth designate as ω_-, is stronger in the ELS data relative to the higher-energy mode ω_+ than in the loss function calculated from reflectivity, but other than that, the calculated and measured spectra are remarkably similar. The discrepancy in intensities probably derives from a small error in the reflectance measurements or Kramers-Kronig (KK) transformation, leading to a small enhancement of ϵ_2 at the minimum, the error being about a factor of 2. We tend to attribute the difference to an error in the reflectivity rather than a difference between the surface and bulk ϵ, since the plasmon energies and shapes are so well predicted, and they would be very sensitive to a change in ϵ.

Feinleib, Scouler, and Ferretti[5] have also provided an accurate dielectric function for ReO_3 derived from optical reflectance data via KK analysis, and have calculated the bulk energy-loss function which is shown in Fig. 3(a). The loss function is very similar to that of the tungsten bronzes except that the interband resonance is shifted about 1 eV to lower energy. Like the bronzes, the agreement with the experimental energy-loss data is exceptionally good, considering that the calculation is for the bulk loss function while the experiment measures the surface loss function. If we assume that the surface-plasmon energies are reduced from the bulk values by about the same amount (~10%) in ReO_3 as in the bronzes, we can expect a similar equivalence between the bulk and surface dielectric functions in ReO_3.

It should be noted that Feinleib *et al.*[5] have suggested a rather different interpretation of the plasmons in ReO_3 than what we have determined from our study of the plasmons in the bronzes as a function of electron density. They note that the higher-energy plasmon peak ω_+ is coincident with the unscreened plasmon energy ω_p, where $\omega_p^2 = 4\pi ne^2/m^*$, which is about 5.5 eV, and assign it to the conduction electron resonance. The lower peak ω_- is assigned to a (hybrid) resonance where the plasmon energy has been depressed due to a strong interaction with the interband resonance. We show in the next section that this interpretation is incorrect.

We conclude that the KK analysis provides an accurate and quantitative description of the bulk dielectric function, and that the bulk and surface dielectric functions are identical. The agreement

between the calculated and observed ω_- energy is within the ELS experimental error in measuring the peak position, ±0.03 eV. Since $\omega_- \propto n^{1/2}$ for small n, where n is the conduction-electron density, we may conclude that the surface electron density is within 5% of the bulk electron density, provided that ω_- is not saturated because of hybridization with the interband transition, as suggested by previous investigators.[5] We discuss this proviso below by means of a model calculation.

B. Model dielectric function for Na_xWO_3

For the purpose of understanding the various roles of screening, mode hybridization, damping or joint-density-of-states bandwidth, and mode interference on the plasmon spectrum we want to construct a simple two-oscillator model for the dielectric function in which one of the oscillators represents the interband polarizability which is conduction-electron-density independent, while the other oscillator represents the conduction-electron polarizability whose strength scales as the electron density n. The latter oscillator is damped by the conduction-electron relaxation rate $\lambda/\hbar$. In order to adequately approximate the shape of the interband contribution to the polarizability, we have allowed for damping such that the damping constant Γ is equal to the full width at half-height of the interband peak in ϵ_2 for $Na_{0.65}WO_3$, which is 2.0 eV. We also include as a third contribution to the polarizability, an energy independent term ϵ_0 which arises from interband excitations whose resonances lie above the range of energies included in our calculation (0–10 eV). This term simply acts to screen the other two terms. Its value is determined selfconsistently with the other parameters from the optical data for $Na_{0.65}WO_3$. Thus we have

$$\epsilon(\omega) = \epsilon_0 - \frac{\omega_p^2}{\omega^2 + i\omega\gamma} + \frac{\Omega^2}{\omega_T^2 - \omega^2 - i\omega\Gamma}. \quad (1)$$

The transverse resonance of the oscillator ω_T is taken to be the first moment of the interband peak, which is 5.2 eV. This is larger by about 0.5 eV than the peak energy because of the skewness of the resonance.

The oscillator strength Ω^2 of the interband resonance is obtained from the relation

$$\Omega^2 = \frac{2}{\pi}\int_0^\infty \omega\epsilon_2(\omega)\,d\omega. \quad (2)$$

To avoid counting twice the conduction-electron polarizability and interband processes above 8 eV, we confined the integration between 3.0 and 8.0 eV. (These limits were also employed in computing the first moment.) We obtain $\Omega^2 = 45$ eV^2.

The other parameters, ω_p, ϵ_0, $\epsilon_s = \epsilon_0 + \Omega^2/\omega_T^2$, and γ, were obtained from a graphical analysis of the optical dielectric data which is given in the Appendix. We find $\omega_p = 5.46x^{1/2}$ eV, $\epsilon_0 = 2.70$, $\epsilon_s = 4.35$, and $\gamma = 0.315$ eV.

One can compute the mean effective conduction-band mass m^* from the value of ω_p established above via the relation $\omega_p^2 = 4\pi ne^2/m^*$. We find $m^* = 0.80m_e$, which agrees well with the value[5] $m^* = 0.86m_e$ found for ReO_3.

It is also interesting to compare the measured energy-loss plasmon linewidth $\gamma = 0.35$ eV with the value $\gamma = 0.315$ eV we obtained in the Appendix from the optical-reflectivity data for the bronzes,[4] and with measured dc conductivities,[15] to determine the energy dependence of γ. γ can be related to τ through $\tau = \hbar/\gamma$ to give, respectively, for 0.35 and 0.315, 1.9×10^{-15} and 2.1×10^{-15} sec. If we compute τ from the dc conductivity σ by the relation $\tau = m^*\sigma/ne^2$, then we obtain for $x = 1$, where[15] $\sigma = 0.88\times10^5$ (ohm cm)$^{-1}$, $\tau = 1.4\times10^{-14}$. However, since σ/n decreases as n decreases, we find that for $x = 0.61$, τ is only 6.7×10^{-15} sec. This is about 3 times longer than the plasmon lifetime, which suggests that interband processes may be important at the plasmon energy in determining γ. For ReO_3, Feinleib *et al.*[5] measure $\sigma = 5.5\times10^4$ (ohm cm)$^{-1}$, which gives $\tau = 8.9\times10^{-15}$ sec, and obtain $\tau = 2.9\times10^{-15}$ sec from their optical data. From our measurement of the conduction-electron plasmon width of $\gamma = 0.60$ eV, we obtain $\tau = 1.1\times10^{-15}$ sec. Thus the dc conduction-electron relaxation times in both the bronzes and in ReO_3 are longer than at the plasmon resonances.

Separating Eq. (1) into its real and imaginary

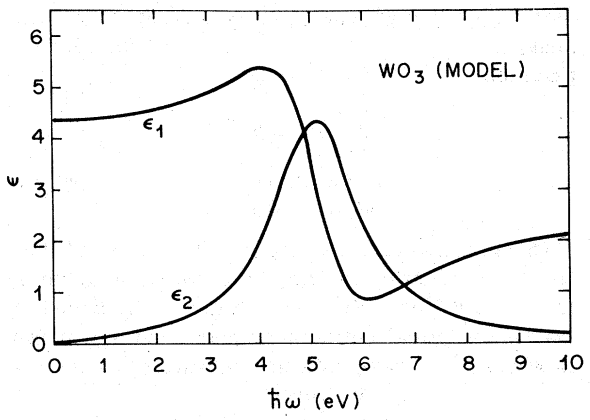

FIG. 4. Contribution of the model interband polarizability to the optical dielectric function. Equation (1) was used with $\omega_p = 0$, and other parameters taken from the optical data as described in the text: $\Gamma = 2.0$ eV, $\omega_T = 5.2$ eV, $\Omega^2 = 45$ eV^2, $\epsilon_0 = 2.70$.

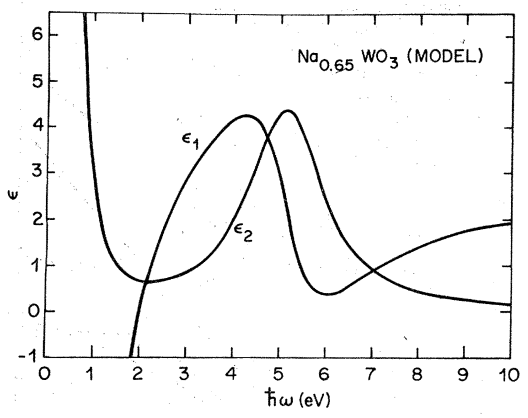

FIG. 5. Model dielectric function for $Na_{0.65}WO_3$. The same parameters were used as for Fig. 4 except that $\omega_p^2 = 19.38$ eV^2, $\gamma = 0.15$ eV.

parts, we have

$$\epsilon_1 = \epsilon_0 - \frac{\omega_p^2}{\omega^2+\gamma^2} + \frac{\Omega^2(\omega_T^2-\omega^2)}{(\omega_T^2-\omega^2)^2+\omega^2\Gamma^2}, \tag{3}$$

$$\epsilon_2 = \frac{\gamma\omega_p^2}{\omega^3+\omega\gamma^2} + \frac{\Omega^2\omega\Gamma}{(\omega_T^2-\omega^2)^2+\omega^2\Gamma^2}. \tag{4}$$

Using the above values for the parameters, except for γ which we took $\gamma = 0.15$ eV (see the Appendix), ϵ_1 and ϵ_2 were calculated and are shown in Figs. 4 and 5. The functions depicted in Fig. 4 correspond to WO_3 with $x = 0$, while those in Fig. 5 correspond to $Na_{0.65}WO_3$. The functions in Fig. 5 represent the optical dielectric function for $Na_{0.65}WO_3$ quite well except for the asymmetry of the interband peak in ϵ_2, and a slight broadening of the interband peak in ϵ_1.

Other than the approximations discussed above, we have also neglected the movement of the Fermi edge relative to the density of unoccupied conduction-band states. This, apparently, causes only small changes in ϵ_2 near the minimum at 2 eV, since the bulk of the oscillator strength comes from transitions to states a few volts above the band edge.

C. Bulk energy-loss function

The bulk energy-loss function is calculated according to

$$\mathrm{Im}(-\epsilon^{-1}) = \epsilon_2/(\epsilon_1^2+\epsilon_2^2). \tag{5}$$

If ϵ_2 varies slowly with energy relative to ϵ_1 the peaks in the loss function will be determined by the zeros in ϵ_1. The zeros in ϵ_1 obtained from Eq. (3) are plotted as the solid line in Fig. 6 as a function of $x^{1/2}$. For small values of x there are one positive real and two positive complex zeros from Eq. (3). The real zero represents the conduction-

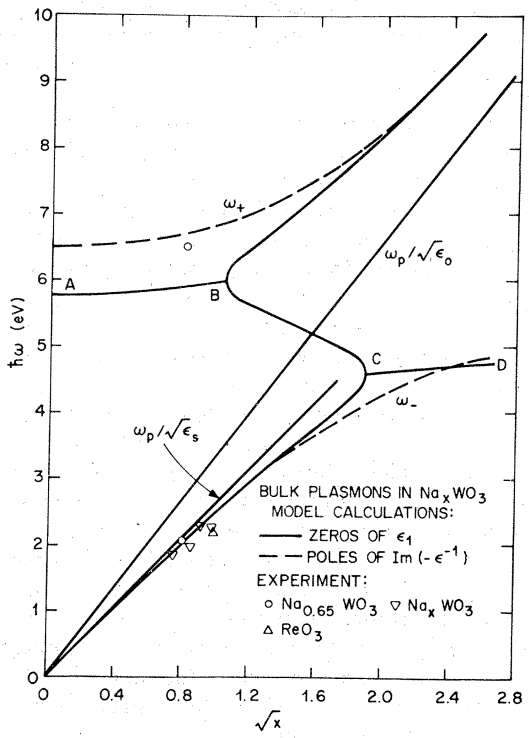

FIG. 6. Comparison of experimental bulk plasmon energies with the model calculation. The inverted triangles refer to x-ray photoemission spectroscopy (XPS) data (Ref. 16), while the other points refer to optical reflectance data (Refs. 4 and 5).

electron plasmon which increases initially in energy linearly with increasing $x^{1/2}$. This branch is asymptotic to $\omega_p/\epsilon_s^{1/2}$ for small values of $x^{1/2}$, since it is screened by the entire interband contribution (in this model) to the static polarizability. The segments AB and CD are the real parts of the complex zeros, and denote the energies of the extrema of ϵ_1. At point B, the aymmetric complex zeros become real positive zeros, since at that point the minimum in ϵ_1 near ω_+ goes negative because of the increasingly negative contribution from the conduction-electron polarizability. Between B and C, the mixing between the plasmon modes becomes important and the upper branch moves rapidly upward in energy, eventually to become asymptotic to $\omega_p/\epsilon_0^{1/2}$ since it is screened only by the high-energy interband polarizability. In this limit, it represents the conduction-electron plasmon again. The other branch eventually saturates at the transverse interband resonance frequency ω_T, but with vanishing intensity.

The important role played by the damping of the interband oscillator, which in our model represents the weighted joint density of states (JDOS), is evident when one plots the peak energies of the loss function. These are given in the figure as the

dashed lines, labeled ω_+ and ω_-. The minimum separation between ω_+ and ω_- is mainly determined by Ω and Γ, while screening due to ϵ_0 tends to push the region of hybridization out to higher-electron densities.

Experimental points for the plasmon peak energies obtained from the optical dielectric function[4] are also plotted on Fig. 6 as circles. It should be noted that these energies were not employed in determining the parameters used in the model dielectric function, so that they constitute another check on the validity of the model.

Excitations have also been observed[16] in XPS spectra as sidebands on the sodium and oxygen *ls* core excitations and on the sodium *KLL* Auger lines, which have been attributed to conduction-electron plasmons. The sideband energies are given as inverted triangles in Fig. 6 which are in good agreement with the calculated bulk plasmon energies within the experimental uncertainties.

The position of the ω_- plasmon determined from optical data[5] in ReO_3 is also given for reference. Since the screening should be about the same in ReO_3 as WO_3, the plasmon energies should scale inversely as the square root of the masses, which accounts for about half of the discrepancy between the ReO_3 point and the curve.

D. Surface energy-loss function

The surface energy-loss function which is obtained from $\mathrm{Im}[-(\epsilon+1)^{-1}]$ is plotted for the model dielectric function [Eq. (1)] in Fig. 7 using the same parameters as for Fig. 6. The solid lines give the zeros of ϵ_1+1, ϵ_1 being given by Eq. (3), with the segments *AB* and *CD* representing the real parts of the complex zeros of ϵ_1+1. The dashed lines give the actual peak energies of the model plasmon spectrum which contains two modes ω_- and ω_+ that are analogous to the modes of the bulk plasmon spectrum. In this case the low-energy branch is asymptotic to $\omega_p/(\epsilon_s+1)^{1/2}$ while the high-energy branch is asymptotic to $\omega_p/(\epsilon_0+1)^{1/2}$. Note that the ratio of the bulk plasmon energy to the surface plasmon energy for low-electron densities is $[(\epsilon_s+1)/\epsilon_s]^{1/2}$ or 1.109, whereas for a free-electron gas the ratio is $\sqrt{2}$.

The effects of hybridization on the surface-plasmon spectrum are identical to the effects obtained by increasing ϵ_0 by 1 in the bulk energy-loss spectrum. In other words, the energy splitting between ω_- and ω_+ is diminished, and the region of hybridization is pushed out to higher electron densities. Note that we distinguish between the effect of mode hybridization which causes the modes to anticross on the configuration diagram (Figs. 6 and 7), and the effects of screening which reduces the slope of the intraband plasmon branch.

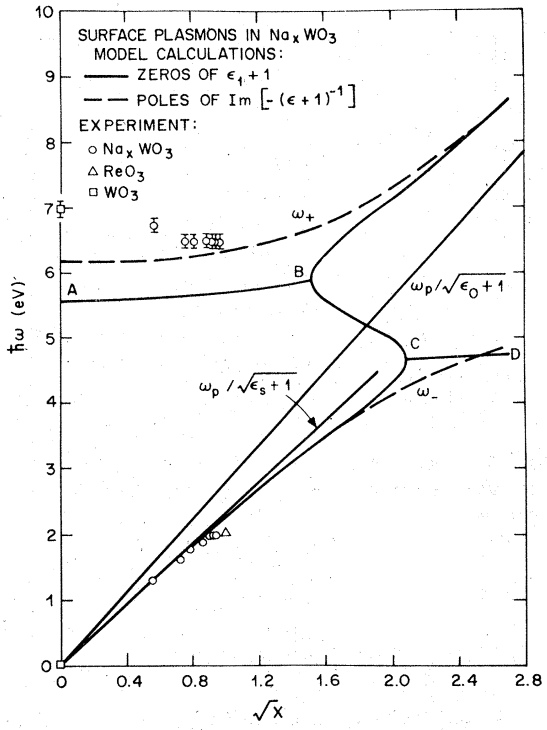

FIG. 7. Comparison of experimental electron-energy-loss data for the surface-plasmon energies with the model calculation.

The latter effect will occur at very low electron densities when the modes are widely separated in energy.

The peak energies found in the experimental energy-loss spectrum are also plotted in Fig. 7. The peak energies are in better agreement with the ω_- surface plasmons than with the analogous bulk plasmons. While one would not expect precise agreement for ω_+ because of the approximations in the interband polarizability, the increasing deviations found at low- or zero-electron density probably derive from structural changes which are sufficient to affect the band structure of these materials.

E. Interference between interacting plasmons

If the polarizability of a system can be represented by a single damped Lorentzian oscillator, then it can be shown that the energy-loss function also contains a Lorentzian line of the same width. For example, in Fig. 8 we plot the full widths at half-height for the bulk plasmon modes calculated from our model dielectric function. This was done by fitting the calculated (model) energy-loss spectrum with a nonlinear-least-squares (NLLSQ) program using two damped Lorentzians. For low-

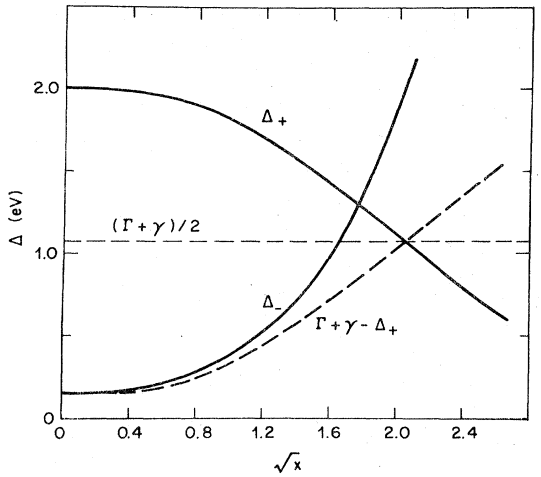

FIG. 8. x dependence of the full width at half-maximum (FWHM) of the bulk plasmon modes obtained from the model calculation. Δ_+ and Δ_- are, respectively, the FWHM values of ω_+ and ω_-. The solid lines give values obtained from a nonlinear-least-squares analysis of the model $\mathrm{Im}(-\epsilon^{-1})$ spectrum. Dashed line gives the values for Δ_- which would be expected if mode interference were absent. As can be seen, the latter effect invalidates the sum rule: $\Delta_+ + \Delta_- = \gamma + \Gamma$ which would be expected from a two-oscillator hybridization model without interference.

electron densities where the plasmons are interacting only weakly, the loss modes have widths equal to the widths of the oscillators in the dielectric function.

As the electron density is increased the modes begin to mix as is evidenced by the change in linewidths. However, the sum of the widths of the lines is not equal to a constant as would be true if the modes were simply mixing without interference. The reason for this asymmetry is given in Fig. 9, where an attempt has been made to fit the model energy-loss spectrum for $x = 1.9$ (corresponding to strong hybridization) with the NLLSQ program using two Lorentzians. The model spectrum shows significant deviations from Lorentzian lineshapes, with constructive interference between the lines, and shifts in the peak positions.

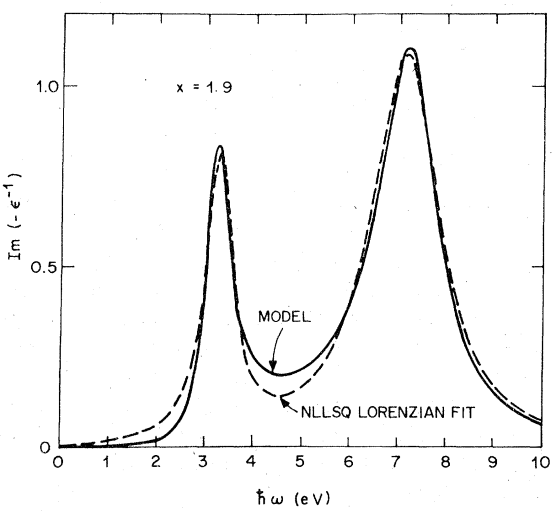

FIG. 9. Effect of mode interference on plasmon line shapes. The solid line gives the energy-loss function for $x = 1.9$, while the dashed line shows a best NLLSQ fit using two Lorentzians.

Thus, we find that a dielectric function consisting of two damped Lorentzians yields an energy-loss function which cannot in general be represented by a superposition of two Lorentzians. There are two exceptions to this rule: The first will hold if the resonances are separated by an energy difference which is large compared to the linewidths, in which case the resonances effectively do not overlap; the second exception is the case of small polarizabilities α; it follows from the fact that $\mathrm{Im}(-1/\epsilon) = \mathrm{Im}[-1/(1+\alpha)] \sim \mathrm{Im}[-(1-\alpha)] = \mathrm{Im}(\alpha)$ for small α. This is probably the case for most core excitations where $\alpha \ll 1$.

Unfortunately our present instrumental resolution does not permit an accurate measurement of the ω_- plasmon line shape, while band-structure effects obscure possible interference effects in ω_+.

F. Some comments on silver metal

We have seen that screening, not hybridization, is the main factor that determines the plasmon energies in the bronzes and in ReO_3. In fact, according to our model which overrepresents mode hybridization due to the long Lorentzian tails of the interband polarizability, ReO_3 and the bronzes with highest-electron density fall near point B on the bulk plasmon diagram (Fig. 6), where hybridization effects are just beginning to become important.

It is interesting that silver metal has a dielectric function[8] that is very similar to that of the bronzes, with a strong interband resonance centered near 5 eV, leading to two interacting plasmon modes, one peaking at 3.8 eV, and the other near 8 eV. Ehrenreich and Phillip[8] have interpreted the upper resonance as being mainly due to the conduction-band plasmon, while the lower plasmon was assigned to a hybrid resonance. While the electron density is somewhat higher in Ag than it is in the bronzes, it is clear that since the minimum in ϵ_1 on the high-energy side of ω_T is still positive, there is only one real zero of ϵ_1, which in Ag falls to the left of point B (see Fig. 6) on its plasmon configuration diagram. Furthermore the width of

the low-energy plasmon is only ~0.2 eV, while the width of the higher energy plasmon is of the order of the interband transition, about 2–3 eV. This indicates that Ag is still well to the left of the crossover region as shown in Fig. 8. These considerations imply that the lower plasmon is mainly derived from the screened conduction-electron polarizability, while the upper plasmon is the screened interband longitudinal resonance.

V. CONCLUSIONS

We have measured the electron-energy-loss functions of Na_xWO_3 for $0 \leq x < 1$, and for ReO_3, and find that they are in excellent agreement with surface loss functions computed from the bulk dielectric function obtained from optical-reflectance data.

We find that hybridization between the plasmon modes is not important for the bronzes and ReO_3, and that the lower-energy plasmon mode is quite well described as the screened conduction-electron resonance. The higher-energy mode is likewise assigned to a relatively unmixed, screened interband resonance, which we find to be essentially independent of electron density over the entire range that is experimentally accessible to Na_xWO_3 $(0 \leq x < 1)$, and to ReO_3.

In order to place the role of plasmon hybridization into perspective in the bronzes and in ReO_3, we have also calculated the loss functions for higher-electron densities where hybridization does become important, and have discussed the effects of screening, damping or JDOS bandwidth, and interference. The latter effect becomes important when the energy separation of the modes is of the same order as the linewidths. Under these conditions we show that the dielectric function and the energy-loss function both cannot be simultaneously represented by a superposition of Lorentzians.

ACKNOWLEDGMENTS

We are grateful to R. L. Campbell for assistance in the measurements, to A. S. Cooper for x-ray measurements of the lattice constants, to W. F. Flood, Jr., who prepared the tungsten crystal, and to D. W. Lynch for making available his tabular data on the optical dielectric function of $Na_{0.65}WO_3$.

APPENDIX: EXTRACTION OF $\epsilon_s, \epsilon_0, \omega_p$, AND γ FROM OPTICAL DIELECTRIC DATA

First we assume that at sufficiently low energies, there are only contributions to the polarizability from the conduction electrons. In that region we have

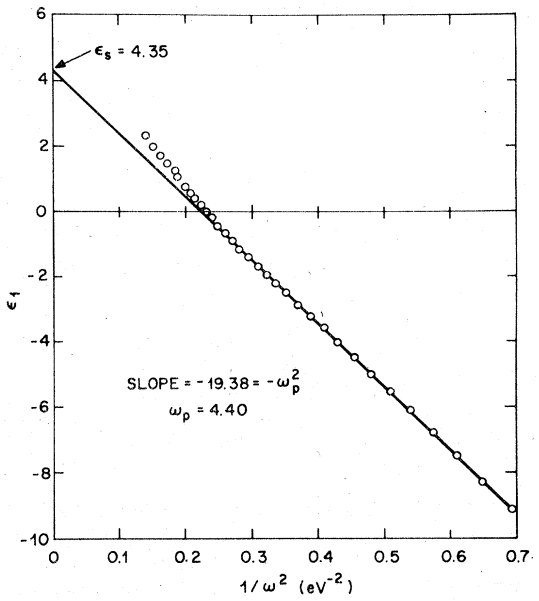

FIG. 10. Technique for obtaining ω_p and ϵ_s from the real part of the optical dielectric function. The data of Ref. 4 were used.

$$\epsilon = \epsilon_s - \omega_p^2/(\omega^2 + i\omega\gamma) \tag{1}$$

where $\epsilon_s \equiv \mathrm{Re}\epsilon(\infty)$ in the usual notation. (ϵ_s represents only the electronic contributions; we need not concern ourselves here with the lattice polarizability).

Separating (1) into real and imaginary parts we have

$$\epsilon_1 = \epsilon_s - \omega_p^2/(\omega^2 + \gamma^2) \tag{2}$$

and

$$\epsilon_2 = \gamma\omega_p^2/(\omega^3 + \omega\gamma^2)\,. \tag{3}$$

From (2) we have for $\omega^2 \gg \gamma^2$,

$$\epsilon_1 \sim \epsilon_s - \omega_p^2/\omega^2\,. \tag{4}$$

Thus a plot of ϵ_1 vs ω^{-2} for $\omega^2 \gg \gamma^2$ should yield a straight line with an intercept equal to ϵ_s and a slope of $-\omega_p^2$. This is shown for the data of Lynch *et al.*[4] for $Na_{0.65}WO_3$ in Fig. 10. For values of $\omega^{-2} > 0.7$ the curve departs from linearity due to the effect of γ. For $\omega^{-2} < 0.25$, there is an abrupt departure due to the interband polarizability. However, in the intermediate region the curve is quite linear, yielding accurate values for $\epsilon_s = 4.35$ and $\omega_p = 4.40$. To obtain a value of ω_p for other values of x we have

$$\omega_p = 4.40(x/0.65)^{1/2} = 5.46x^{1/2}\ \text{eV}\,. \tag{5}$$

While one can estimate the value of γ by fitting Eq. (2) for $\omega^{-2} > 0.7$, we find that γ is rather ener-

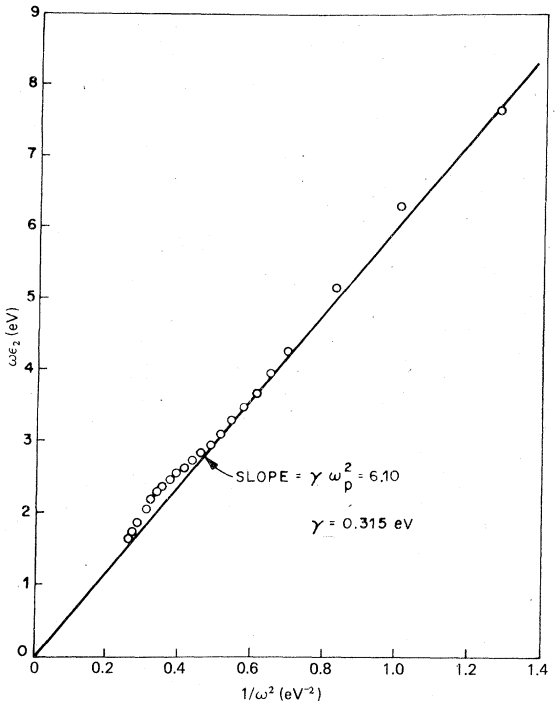

FIG. 11. Technique for obtaining γ from the imaginary part of the optical dielectric function, using the data of Ref. 4, and ω_p^2 obtained from Fig. 10.

gy dependent when obtained by this procedure, which produces values between 0 and 0.3. In the calculations given in the discussion section, we used a mean value of 0.15 eV for γ. However, subsequent to making the calculations of the loss function, we attempted to estimate γ from ϵ_2, since by so doing we could make use of the higher-energy optical data which may be more accurate. This was done by rewriting Eq. (3) to avoid the singularity in ϵ_2 at zero frequency,

$$\omega\epsilon_2 = \gamma\omega_p^2/(\omega^2+\gamma^2)\,. \tag{6}$$

Then for $\omega^2 \gg \gamma^2$, one can plot $\omega\epsilon_2$ vs ω^{-2}, and obtain a straight line passing through the origin whose slope is $\gamma\omega_p^2$. This is done in Fig. 11 for the optical ϵ_2 data from $Na_{0.65}WO_3$. While there appear to be some weak interband processes in this region, the data do nicely establish a line passing through the origin with a slope of 6.10 eV^3. From the value of the slope of Fig. 11, we obtain γ = 0.315 eV. This number compares well with the widths of the bulk and surface plasmons obtained from the optical data, γ = 0.29 eV.

Having found a value for ϵ_s, we must now find ϵ_0. This is done by subtracting from ϵ_s the zero-frequency interband polarizability:

$$\epsilon_0 = \epsilon_s - \Omega^2/\omega_T^2 = 2.70\,. \tag{7}$$

---

*Permanent address: Institut fur Festkorperforschung der Kernforschungsanlage, Postfach 1913, D-5170 Julich 1, West Germany.

†Permanent address: Laboratoire PMC, Ecole Polytechnique, Route de Saclay, 91120 Palaiseau, France.

[1]T. Iwai, J. Phys. Soc. Jpn. 15, 1596 (1960).

[2]M. Campagna, G. K. Wertheim, H. R. Shanks, F. Zumsteg, and E. Banks, Phys. Rev. Lett. 34, 738 (1975).

[3]R. Clarke (private communication).

[4]D. W. Lynch, R. Rosei, J. H. Weaver, and C. G. Olson, J. Solid State Chem. 8, 242 (1973).

[5]J. Feinleib, W. J. Scouler, and A. Ferretti, Phys. Rev. 165, 765 (1967).

[6]C. B. Wilson, Proc. Phys. Soc. 76, 481 (1960).

[7]D. W. Lynch (private communication) has supplied us with tabular data for the dielectric function, from which Figs. 2(a) and 2(b) were prepared.

[8]H. Ehrenreich and H. R. Philip, Phys. Rev. 128, 1622 (1962).

[9]J. M. Berak and M. J. Sienko, J. Solid State Chem. 2, 109 (1970).

[10]B. W. Brown and E. Banks, J. Am. Chem. Soc. 76, 963 (1954).

[11]H. R. Shanks, J. Cryst. Growth 13/14, 433 (1972).

[12]R. A. Phillips and H. R. Shanks, Phys. Rev. B 4, 4601 (1971).

[13]J. J. Ritsko, H. Witzke, and S. K. Deb, Solid State Commun. 22, 455 (1977).

[14]L. F. Mattheiss, Phys. Rev. 181, 987 (1969).

[15]I. Webman, J. Jortner, and M. H. Cohen, Phys. Rev. B 13, 713 (1976).

[16]J.-N. Chazalviel, M. Campagna, G. K. Wertheim, and H. R. Shanks, Phys. Rev. B 16, 697 (1977).